Submicron-Sampling of Living Cells by Macrophages

Authors: Amy C. Fan[1,*], Rukman Thota[1,*], Nina Serwas[1,*], Kyle Marchuk[2], Megan Ruhland[1], Austin Edwards[2], Matthew F. Krummel[1,‡]

---

[1]Department of Pathology, University of California San Francisco, San Francisco, CA 94143, USA,

[2]Biological Imaging Development CoLab, University of California, San Francisco, CA 94143, USA.

[*] These authors contributed equally to this work.

[‡]Lead Contact, email: matthew.krummel@ucsf.edu

SUMMARY PARAGRAPH

An effective immune system must sample and appreciate healthy-self identity to prevent autoimmunity and to contrast to pathogenic insults[1–3]. Self-proteins are presented to T cells in the thymus during immune cell development[2,3], and must be presented throughout the body to both maintain regulatory T cell populations[4–6] and provide a tonic signal to maintain conventional T cells over time[7–9]. The ready observations of continuous apoptosis in some organs together with the ingestion of that material by myeloid populations has led to a conventional understanding of ongoing cell-death as a major source of self-antigens[10], complemented in some situations by uptake of free-floating cell-derived vesicles. Here, we used a series of companion imaging and vesicular labeling technologies to reveal an alternate process undertaken by macrophages that results in non-destructive and direct sampling of living cells. The process requires cell-cell contact, does not require caspase activation, and takes place via a trogocytosis-like stretching of the target cell into the macrophage, leading to the generation of submicron-sized vesicles containing cytoplasm. Using a high-dimensional flow-based method for labeling vesicles ingested under this versus other conditions, we find that live-sampled material is distinctly processed, is poorly subject to fusion with lysosomes, and produces ensuing differential effects on the presentation of those to CD4 versus CD8 T cells. This demonstrates an important and substantial sampling of living cells by the immune system, with clear consequences for maintaining the border of immunity.

39 **MAIN**

40 **Tissue and tumor-associated proteins are routinely sampled by myeloid cells**

41 Antigen presenting cells (APCs) must continuously survey tissues by ingesting and processing antigens for
42 presentation to direct antigen-specific T cell responses[11]. In the course of studying a selection of tissue-
43 specific sites of tolerance, including in tumors, we expressed the fluorescent protein ZsGreen in multiple
44 non-inflammatory settings across a range of tissues with slow turnover rates (Scbg1a1-Cre-ERT2; airway
45 epithelium)[12] or faster turnover (K14-Cre skin, tumors, Villin-Cre intestinal epithelium). ZsGreen is both
46 bright and very stable, permitting superior long-lived tracking[1,10,24]. Cytosolic ZsGreen expressed under
47 these promoters all routinely illuminated substantial $CD45^+$ immune populations that contained numerous
48 submicron-sized vesicular puncta of ZsGreen (**Fig. 1a, b)**, consistent with ingestion of tissue-associated
49 protein. When $CD45^+$ cells bearing $ZsGreen^+$ were isolated from these healthy tissues, a variety of myeloid
50 cells were highlighted (**Fig. 1c, d; Extended Data Fig. 1a,b; Supplementary Fig. 1**), including dendritic
51 cells and neutrophils but with macrophages being the most consistently loaded. These loading frequencies
52 also mirror previous characterization of myeloid sampling of skin[13] and tumor cytoplasts[14].

53

54 These observations do not result from misexpression of transgenes in host tissues as demonstrated by the
55 following series of observations. First, we compared the ZsGreen fluorescence intensity of lung myeloid
56 cells in mice expressing ubiquitous ZsGreen ("B-actin-Cre;ZsGreen"), lung-specific ZsGreen ("Scgb1a1-
57 Cre-ERT2;ZsGreen"), or no ZsGreen (C57BL/6 wildtype, "B6 WT"). In each myeloid cell population,
58 ZsGreen fluorescence intensity in the Scgb1a1-Cre-ERT2;ZsGreen mice was greater than in B6 WT mice
59 but less than in B-actin-Cre;ZsGreen mice (**Extended Data Fig. 1b**), consistent with accumulation of
60 exogenous ZsGreen protein as opposed to cell-autonomous ZsGreen expression. Second, normal bone-
61 marrow transplanted into mice expressing ZsGreen gave rise to donor-derived myeloid cell populations that
62 were bright for ZsGreen (**Extended Data Fig. 1c; Supplementary Fig. 2a**). Third, in mice ubiquitously
63 expressing TdTomato transplanted subcutaneously with B16F10 tumors expressing ZsGreen ("B16-

ZsGreen"), host CD45^{+} immune cells contained tumor-derived vesicular ZsGreen puncta and a significant proportion of tumor-associated myeloid cells ingested ZsGreen (**Fig. 1e,f, Supplementary Fig. 2b**). Finally, whereas we had previously observed trafficking of tissue-specific ZsGreen to tissue draining lymph nodes[13], ZsGreen was not detected in the non-draining lymph node of Scgb1a1-Cre-ERT2;ZsGreen mice (**Fig. 1g**), indicating tissue-specific uptake.

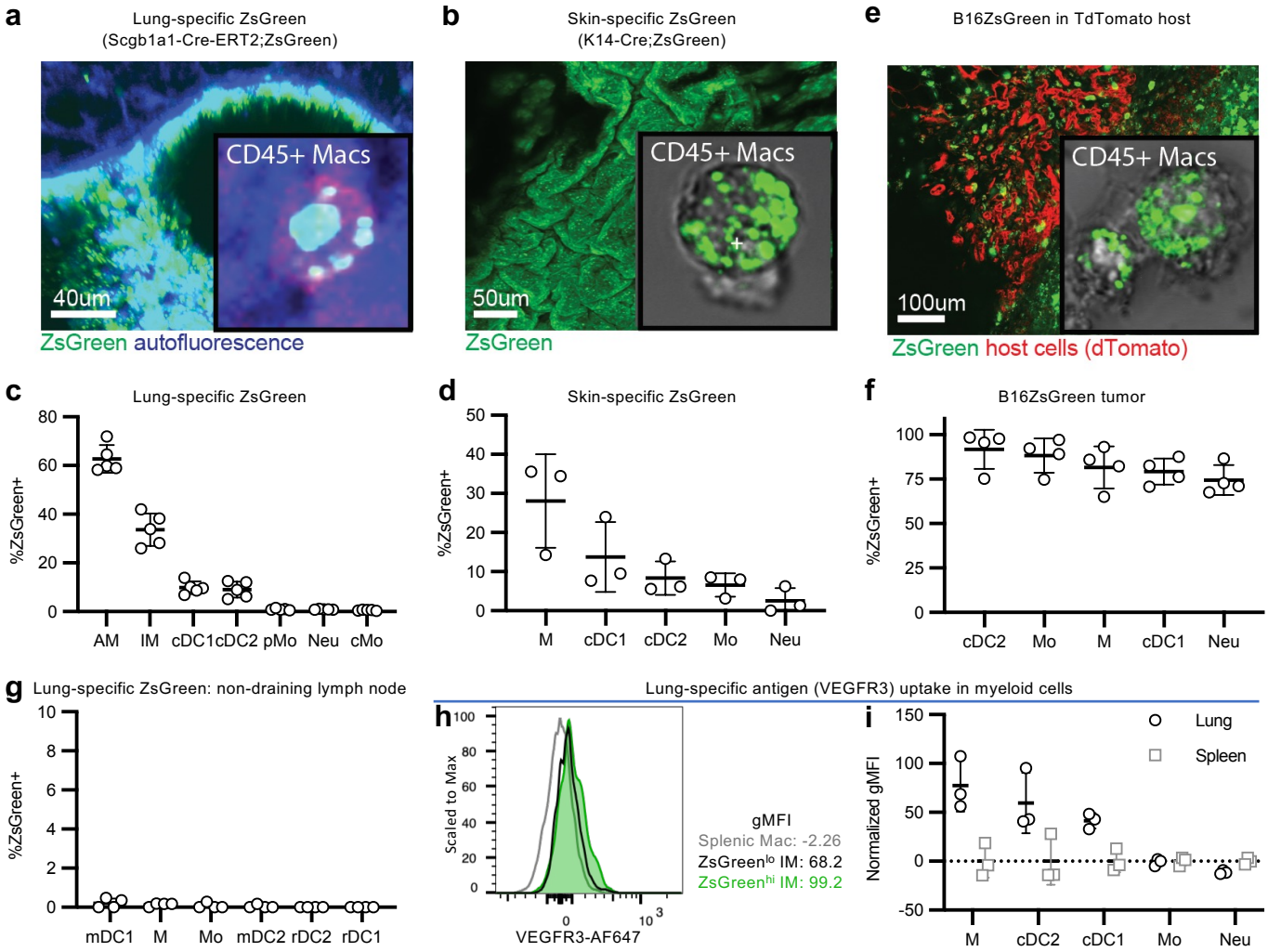

Figure 1: Myeloid cells sample proteins from healthy and tumor tissues

a-b, Lungs (**a**) or skin (**b**) taken from mice expressing ZsGreen under the Scgb1a1 (**a**) or K14 (**b**) Cre with insets of in situ macrophages labeled with CD45 (**a**) or sorted CD45+ Macrophages (**b**) showing ZsGreen puncta inside macrophages. **c-d,** Isolation of lung myeloid cells from Scgb1a1-Cre-ERT2;ZsGreen mice (**c**) or skin myeloid cells from K14-Cre;ZsGreen mice (**d**) shows specific uptake in tissues prominently in macrophages. Lymphocytes were routinely ZsGreen negative. **e,** B16 melanoma cells expressing ZsGreen transplanted into mice ubiquitously expressing TdTomato with inset of CD45+ macrophages. **f**, Isolation of tumor-associated myeloid cells shows broad uptake of ZsGreen across myeloid cell subsets. **g**, Isolation of inguinal LN myeloid cells from Scgb1a1-Cre-ERT2;ZsGreen mice shows no uptake in distant lymph nodes. **h,** Intracellular staining for airway specific VEGFR3 protein in lung (black) compared to splenic (gray) myeloid cell populations with ZsGreen^{hi} lung macrophages (green) further enriching for VEGFR3 signal. **i,** VEGFR3 MFI in lung and splenic myeloid cell populations normalized to average MFI of splenic myeloid cells. Representative of 3 experiments, n = 3-6 mice per experiment. AM, alveolar macrophage; IM, interstitial macrophage; pMo, patrolling monocyte; Neu, neutrophil; cMo, conventional monocyte; M, macrophage; Mo, monocyte, mDC2, migratory cDC2; mDC1, migratory cDC1; rDC1, residential cDC1; rDC2, residential cDC2

84 For tumor antigens, it was previously found that tumor antigens were co-packaged in macrophage vesicles,
85 together with tumor-derived ZsGreen tracer[13]. To determine if other non-tumor self-antigens in healthy
86 tissues with low turnover like epithelium were similarly taken up in these myeloid cell populations, we
87 examined the levels of VEGFR3 and PLVAP proteins, which are specifically expressed on the cell surface
88 of non-hematopoietic cells in the lung. When we examined the cellular components from the lungs of
89 Scgb1a1-Cre-ERT2;ZsGreen mice by intracellular flow-cytometry, we found that local myeloid cell
90 populations from the lung, but not distant splenic myeloid cells, contained these self-proteins **(Fig. 1h, i;**
91 **Extended Data Fig. 1d; Supplementary Fig. 2c)**. Further, ZsGreen^{hi} myeloid cells were brighter for the
92 VEGFR3 and PLVAP stains as compared to ZsGreen^{lo} myeloid cells (**Fig. 1h; Extended Data Fig. 1d**).
93 Therefore, tissue-associated myeloid cells regularly sample tissue-associated self-proteins, both normal and
94 tracer.
95
96 **Substantial antigen sampling from live cells by macrophages**
97 Several mechanisms of uptake might contribute to myeloid cell sampling from tissues in vivo, with the most
98 heavily studied to date being phagocytosis and endocytosis. To formally interrogate how myeloid cells can
99 obtain intracellular material from nearby cells, we established an in vitro assay for sampling using donor
100 cell populations, grown at ~99% viability, in log phase. We co-cultured bone marrow derived macrophages
101 (BMDMs) with those ZsGreen-expressing target, especially focusing on two model target cells: B16-
102 ZsGreen melanoma cells which in these conditions minimally produce exosomes, or primary mouse
103 embryonic fibroblasts isolated from mice ubiquitously expressing ZsGreen ("MEF-ZsGreen"). From this
104 co-culture, we detected significant ZsGreen^{+} uptake from both target cells into the BMDM, with the
105 intensity of that ZsGreen being hundreds of times lower than the intensities of intact donor cells, consistent
106 with partial sampling as opposed to complete engulfment (**Fig. 2a, Supplementary Fig. 3**). When those
107 ZsGreen^{+} BMDMs were sorted for imaging by high-resolution spinning disk confocal microscopy, we
108 readily visualized internalized submicron-sized ZsGreen^{+} puncta (**Fig. 2b; Extended Data Fig. 2a, b**).

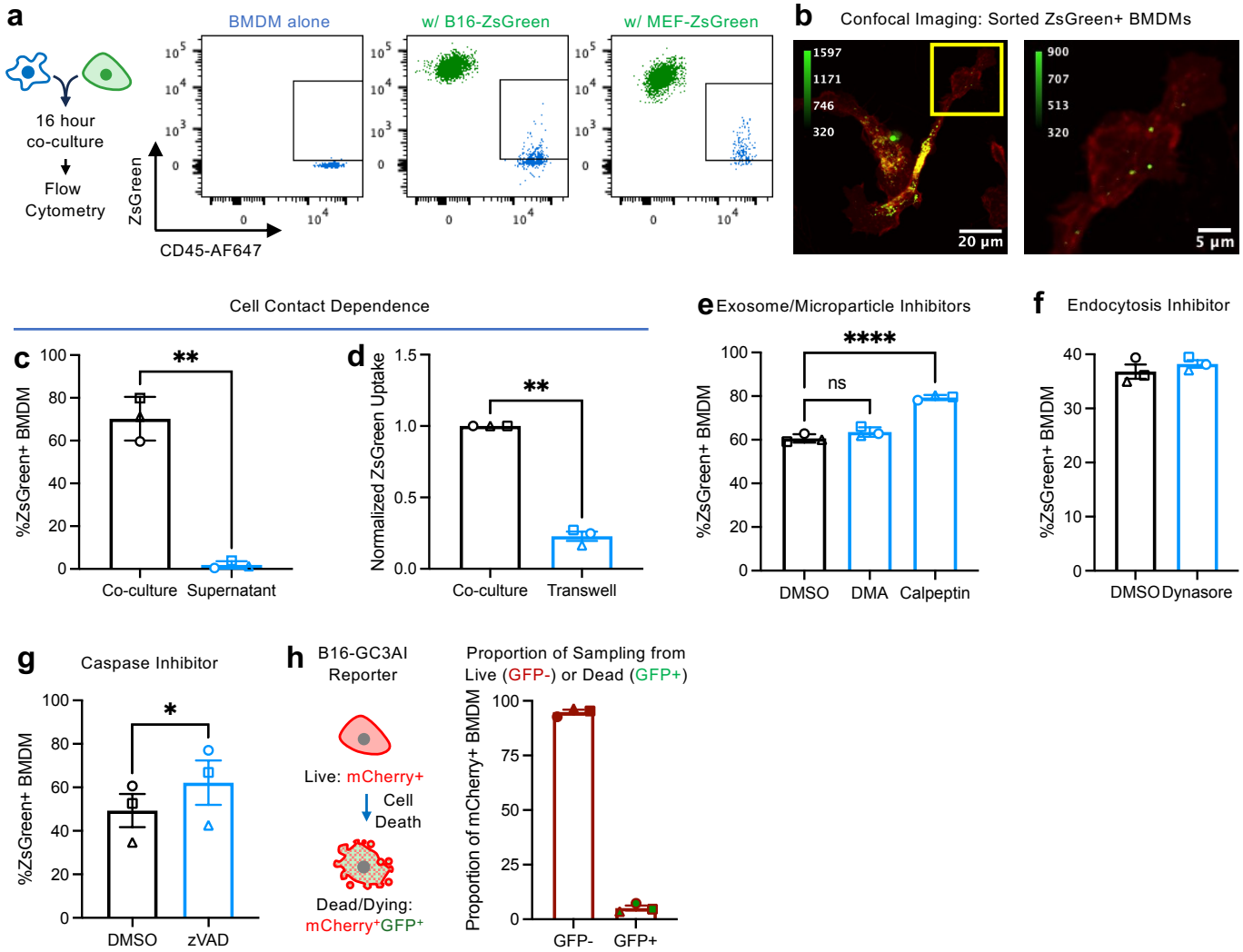

Figure 2: Live cells can be sampled in a cell-contact dependent manner without caspase activation
a, BMDMs and ZsGreen-target cells are co-cultured for 16 hours prior to evaluation for ZsGreen uptake by flow cytometry. **b**, Sorted ZsGreen$^+$ BMDMs with membrane Tomato showcasing ZsGreen$^+$ puncta. **c-d**, BMDMs were co-cultured directly with B16s, with B16 supernatant (**c**), or with a transwell insert containing B16s (**d**). **e-g**, In vitro co-cultures were treated with indicated inhibitors or DMSO vehicle control. **h**, BMDM co-culture with B16-F10 expressing GFP caspase 3 activity indicator (B16-GC3AI) demonstrates uptake is predominantly from live mCherry$^+$GFP$^-$ target cells. n = 3 biological replicates. Shown are mean of technical replicates +/- s.e.m. One-way ANOVA or paired t-test. * $p < 0.05$, ** $p < 0.01$.

We then evaluated whether antigen sampling from live cells in this setting is mediated through uptake of soluble particles and/or was cell-contact dependent, where the former in particular is expected for the ingestion of free exosomes and perhaps apoptotic blebs. Culture of BMDMs with either B16-ZsGreen derived supernatant containing the limited number of exosomes produced in a 48-hour period or B16-ZsGreen cells that were separated from the BMDM by a transwell both significantly reduced uptake (**Fig. 2c, d; Extended Data 2c**). Additionally, treatment of cultures with inhibitors of either exosome/microparticle release or endocytosis both did not reduce uptake (**Fig. 2e, f; Extended Data 2d,**

126 **e**). Therefore, although endocytosis of soluble material such as exosomes and microparticles may contribute
127 modestly, this suggested a distinct dominant mechanism of uptake of live cell-associated material in this
128 setting, requiring cell-contact.
129
130 Since an existing paradigm suggests that phagocytosis of apoptotic bodies, termed efferocytosis but
131 heretofore just "phagocytosis", is the major mechanism by which tissues donate material to surveilling
132 APCs[15–17], we sought to test whether cell death is necessary for the substantial sampling in our system.
133 When we treated the co-culture with the caspase inhibitor zVAD, we found no effect upon ZsGreen uptake,
134 a result which does not support that this uptake relies on cell death (**Fig. 2g**, **Extended Data Fig. 2f**). To
135 study more directly whether the material ingested into macrophages came from cells undergoing apoptosis,
136 we used a B16-F10 model cell line expressing constitutive mCherry and a split GFP caspase 3 activity
137 indicator which fluoresces only when cleaved, as during apoptosis[18] ("B16-GC3AI") (**Fig. 2h**). Use of this
138 confirmed that the B16-GC3AI cells that went into our assays were highly viable (0.12% GFP^+), whereas
139 apoptotic cell death induced by Staurosporine resulted in GFP reporter fluorescence (>63% GFP, **Extended**
140 **Data Fig. 2g**). When these reporter-expressing cells were co-cultured with BMDM, we found that the
141 majority of the Cherry-positive cells (those that had taken up material from the donor cells) lacked GFP
142 expression compared to uptake following apoptosis (1% for live sampling **Fig. 2h,** versus 11% following
143 staurosporine **Extended Data Fig. 2h)**. Together, these results further support that an alternative sampling
144 pathway, beyond those involving apoptosis, exists for obtaining material from live cells.
145
146 **Live-Imaging of Live-sampling**
147 Given the small size of particles we found within macrophages, we adopted high-resolution methods to
148 directly image the time-course of B16-ZsGreen cells interacting with BMDMs expressing membrane-
149 TdTomato in a co-culture. We variously used lattice light sheet imaging with isotropic resolution of
150 approximately ~220nm, or the Nikon Spatial Array Confocal (NSPARC), detector system which utilizes an

151 ultra-low noise detector array with approximate lateral and axial resolutions of approximately ~212nm and
152 ~424nm, respectively. Importantly, both technologies can sample live full cell volumes over time with
153 reduced phototoxicity.
154
155 Using NSPARC, we observed target cell-BMDM interactions that spontaneously result in the stretching of
156 a protrusion of the target cell into the BMDMs. This was frequently followed by the separation of a distinct
157 ZsGreen^{+} vesicle (**Fig. 3b**). In a representative movie (**Fig. 3b and supplemental movie 1**), this entire
158 process took <10 minutes from imaging of the initial ZsGreen^{+} protrusion until the time when a protrusion
159 was no longer visible from the target cell, although we registered the actual abscission of the vesicle within
160 a single frame (30 seconds; **Fig. 3a, b**) followed by complete loss of the remaining tether, either into the
161 vesicle or back into the donor cell. We confirmed, at the end of the process, that very small amounts of
162 target cell material were physically inside the BMDM by analyzing the same data in YZ and XZ projections
163 (**Extended Data Fig. 3a**). Consistent with the size ranges we have observed in vivo[13], these separated
164 vesicles were small, ranging from diffraction limited (<~0.02μm^3) to ~0.05μm^3 (**Fig. 3c**). In some cases,
165 we also saw a protrusion pulled into the BMDM but then retracted without detectable pinching of a vesicle,
166 which might either have led to extremely tiny ingestion or was simply abortive. Post-ingestion, ZsGreen^{+}
167 puncta moved within the cytoplasm (**Extended Data Fig. 3b**). These data suggest that live-cell cytosolic
168 material can be sampled in a contact-dependent, trogocytosis-like manner.
169
170 To confirm that this process was not an artefact of the detection method and to take advantage of faster
171 frame-rates, we also leveraged lattice light sheet (LLS) microscopy[19] with its isotropic high resolution,
172 which again captured the stretching and separation of ZsGreen^{+} vesicles, this time again visible across a
173 single frame (now ~8 seconds; **Fig. 3d, Extended Data Fig. 3d**). Although ingested vesicles were
174 occasionally identified using spinning disk confocal (**Extended Data Fig. 3c**), it is possible that the small
175 size of these vesicles (limiting total fluorescent yield) and the lower sampling rate of this ingestion method

limits our ability to capture this biology with older technologies. This also provides one possible explanation why this process has not yet been described or extensively studied by conventional microscopic methods.

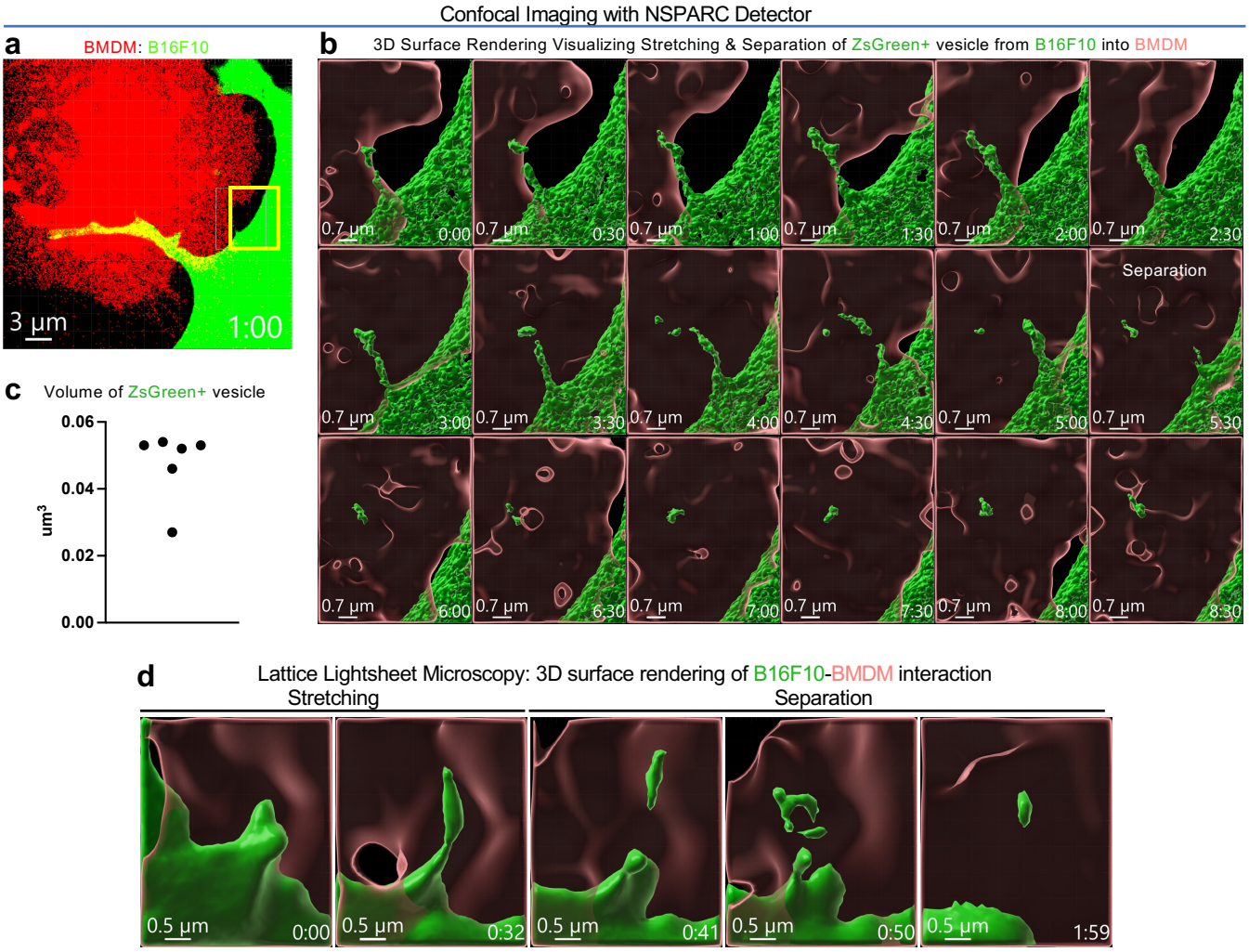

Figure 3: Trogocytosis-like sampling enables macrophages to ingest cytosolic protein from live cells
a-b, Confocal live imaging of TdTomato$^+$ BMDM and ZsGreen$^+$ B16F10 interactions using the NSPARC detector. Time shown as m:ss. **a,** Two-color volume rendering displaying interaction between TdTomato$^+$ BMDM and ZsGreen$^+$ B16F10. Yellow box highlights the region of interest displayed in **(b). b,** Three-dimensional surface rendering from ROI in **(a)** visualizing the formation and separation of a vesicle from ZsGreen+ B16 into TdTomato+ BMDM. Z-stacks within series were captured in 30 sec intervals. **c,** Volume measurements of separated vesicles from frames 13-18 in **(b)** using Imaris object statistics. **d,** Lattice light-sheet imaging of TdTomato$^+$ BMDM and ZsGreen$^+$ B16F10 capturing the stretching and separation of ZsGreen$^+$ vesicle from target cell. Time shown as m:ss.

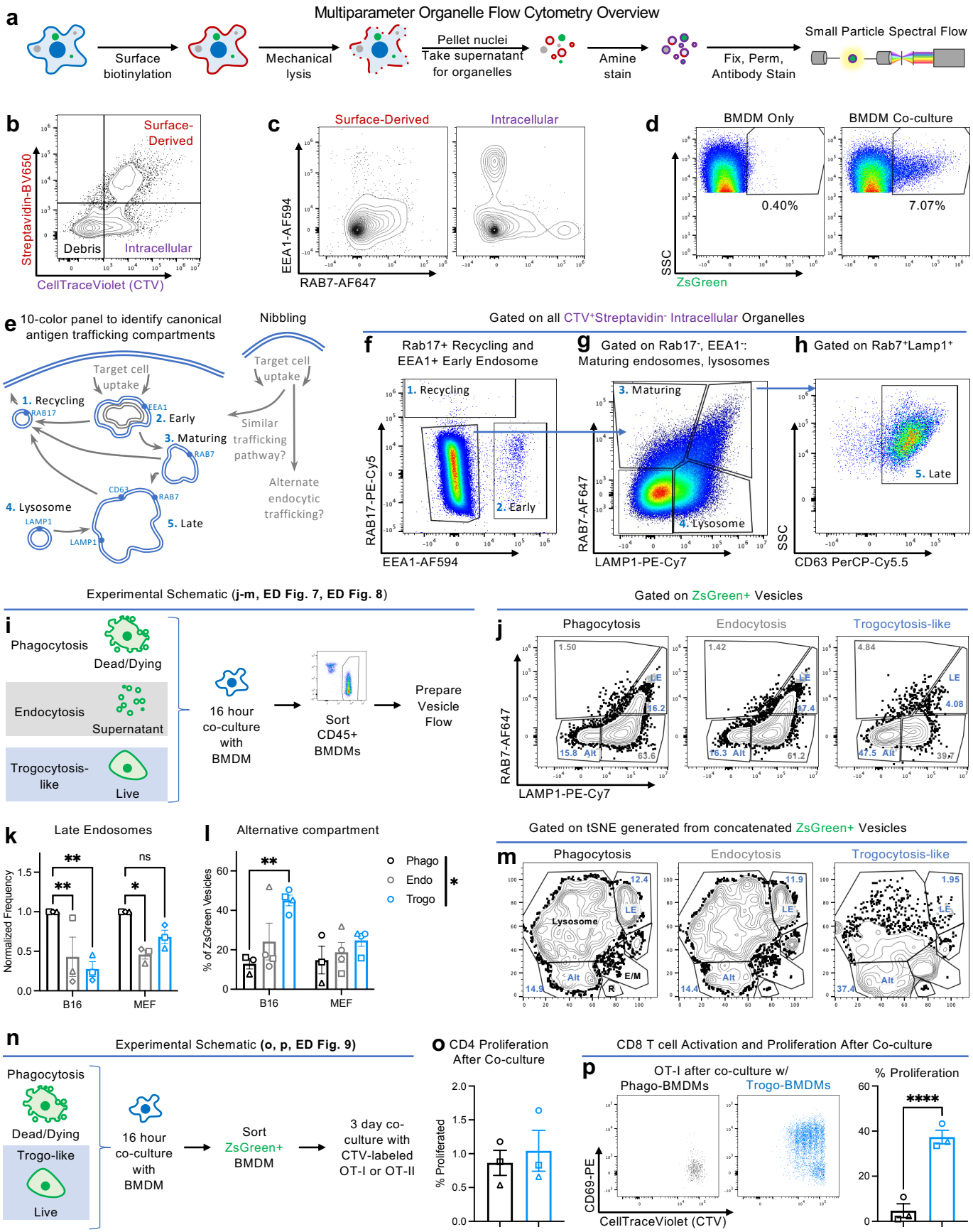

Figure 4: Multiparameter intracellular vesicle flow cytometry reveals that live-cell associated protein fills a discrete vesicular compartment

a, Cell surface membrane is biotinylated prior to mechanical lysis and low-speed centrifugation. Supernatant containing organelles are stained with CellTraceViolet, fixed, permed, and stained with antibodies against vesicle-associated antigens. **b,** Discrimination of Strepavidin^{-} CellTraceViolet^{+} intracellular, protein-containing particles. **c,** Vesicle-staining antibodies primarily stain intracellular particles. **d,** Discrimination of ZsGreen+ vesicles allows for tracking of vesicles containing target-cell-derived protein. **e-h,** Identification of vesicle compartments by vesicle flow panel. **i,** Experimental schematic to evaluate trafficking downstream of different sampling mechanisms. **j-m,** Representative flow plots (**j**) or tSNE (**m**) of ZsGreen^{+} vesicles derived from different sampling mechanism with summary quantification of proportion of ZsGreen+ vesicles in late endosome (**k**) and alternative compartment (**l**). **n,** Experimental schematic to evaluate T cell activation downstream of different sampling mechanisms. ZsGreen^{+} BMDMs were sorted after co-culture with live or apoptotic B16F10-ZsGreen-minOVA target cells and subsequently co-cultured with CellTraceViolet (CTV)-labeled OT-I CD8+ or OT-II CD4+ T cells in a 1:3 BMDM:T ratio for 3 days. **o,** Proliferation of OT-II CD4 T cells as read out by loss of CellTraceViolet after 3 days of co-culture with ZsGreen+ BMDMs that ingested material using phagocytosis (black) or trogocytosis-like (blue) mechanisms. **p,** Activation and proliferation of OT-I CD8 T cells as read out by CD69 expression or loss of CellTraceViolet after 3 days of co-culture with ZsGreen+ BMDMs from phagocytosis (black) or trogocytosis (blue) conditions. n = 3-4 biological replicates. Shown are mean of technical replicates +/- s.e.m. One-way ANOVA or paired t-test.

Antibody opsonization and integrins amplify cell-sampling

Although it is likely that a process such as this can be mediated by multiple receptor-ligand interactions, we sought to determine whether previously described mechanisms such as antibody-opsonization can augment this cell sampling (**Extended Data Fig. 4a**). To this end, we found that, antibodies to two surface proteins (CD29 and CD98) both increased ZsGreen uptake (**Extended Data Fig. 4b, c**). Similarly, pre-incubation of ZsGreen target cells with normal mouse serum or isolated IgG prior to co-culture with BMDMs increased ZsGreen uptake (**Extended Data Fig. 4d,e),** suggesting that even weakly cross-reactive collections of antibodies amplifies sampling from live cells. Furthermore, we found that disruption of complement receptor CR3 (CD11b but not CD18) in BMDM decreases the frequency and intensity of ZsGreen uptake in B16 and MEFs (**Extended Data Fig. 5**), similar to findings that synaptic pruning by microglia involves these receptors[20].

Tracking sampled material using high-dimensional intracellular vesicle flow cytometry

We sought to determine whether this mechanism has any distinct functional downstream consequences for the vesicle or cargo by first interrogating its fate as compared to material obtained by phagocytosis or endocytosis. To facilitate a high-dimensional analysis of the organelles that derived from different modes of cell sampling, we developed a 10-parameter flow-based organelle profiling method, loosely based on a

225 previous phagoFACS[21], here capable of immunophenotyping of multiple intracellular compartments (**Fig.**
226 **4a**, see **Methods**). Importantly, we incorporated a cell-surface biotinylation step prior to lysis, to allow
227 definitive discrimination of surface-derived membrane, and we also stained the preparation with amine-
228 binding CellTraceViolet to focus analysis upon protein-associated intracellular organelles (**Fig. 4b**,
229 **Extended Data Fig. 6a,** see **Methods**). Reassuringly, markers for intracellular organelles such as Early
230 Endosome Antigen 1 (EEA1) and RAB7 are exclusively detected in the streptavidin-negative material (**Fig.**
231 **4c**). In CellTraceViolet^{+} intracellular vesicles isolated from BMDMs, we were able to distinguish ZsGreen^{+}
232 antigen-containing vesicles from ZsGreen^{-} antigen-free vesicles, and these were exclusively found in
233 BMDMs that had been co-cultured with ZsGreen-expressing target cells (**Fig. 4d, Extended Data Fig. 6b**).
234
235 Vesicles derived from internalization are understood to flow through a pathway consisting of progressively
236 more degradative compartments; early endosomes mature into late endosomes that fuse with lysosomes to
237 form phagolysosomes[10,22]. We tuned our panel to identify known vesicular compartments, including
238 RAB17^{+} recycling endosomes, EEA1^{+} early endosomes, LAMP1^{+} lysosomes, RAB7^{+} maturing endosomes,
239 and RAB7^{+}LAMP1^{+}CD63^{+} late endosomes (**Fig. 4e-h**). By further incorporating antibodies recognizing
240 antigen presentation molecules major histocompatibility complex (MHC) I and II, we could identify
241 compartments consistent with antigen-loading. Consistent with previous reports[10], MHC I is primarily
242 excluded from LAMP1^{+} vesicles whereas MHC II can be detected across multiple vesicular compartments
243 (**Extended Data 6b**). Together, these results highlighted the suitability of a high-dimensional vesicle
244 analytic method to study composition and identity of vesicular compartments.
245
246 We then applied this organelle immunophenotyping method to compare the intracellular trafficking of
247 ZsGreen^{+} antigen-containing vesicles after trogocytosis-like live-sampling to other sampling mechanisms,
248 including endocytosis and phagocytosis (**Fig. 4i**). While endocytosis of soluble material derived from
249 supernatant resulted in very low levels of ZsGreen uptake (**Extended Data Fig. 7a, b**), sufficient ZsGreen

250 vesicles were nevertheless detectable for downstream analysis. In a conventional gating analysis, both
251 phagocytosis and endocytosis resulted in distributions of proteins across the vesicle maturation spectrum,
252 but revealed decreased trafficking of vesicles resulting from trogocytosis-like sampling to the late endosome
253 (**Fig. 4j,k, Extended Data Fig. 7b,c**) and target cell-dependent changes in the co-localization of these with
254 MHC-I but not MHC II (**Extended Data Fig. 7d**). Notably, while ~90% of ZsGreen^{+} vesicles resulting
255 from phagocytosis were associated with a conventional vesicle marker, a substantial portion of ZsGreen+
256 vesicles resulting from live-sampling did not associate with these canonical endocytic markers (**Fig. 4l**).
257 This suggested the sequestration of live-sampled material into an alternative endocytic trafficking pathway,
258 rather than those associated with degradation.
259
260 To analyze vesicle populations based on their intensity for each of our markers and in a way unbiased by
261 previous classifications, we displayed the concatenated ZsGreen+ vesicles in a t-distributed stochastic
262 neighbor embedding (tSNE) plot using only the vesicle protein marker intensities as parameters (**Extended**
263 **Data Fig. 8a,b**). This demonstrated that while vesicles derived from each sampling method overlapped,
264 there was a distinct shift in the distribution of vesicles comparing live-sampling (trogocytosis-like), to
265 conventional phagocytosis of apoptotic cells (**Fig. 4m, Extended Data Fig. 8b**). When we overlayed
266 intensities of markers such as LAMP1 and consistent with the conventional flow gating strategy, vesicles
267 resulting from live-sampling were relatively depleted in late endosomes and enriched in an alternative
268 vesicular compartment (**Fig. 4m, Extended Data Fig. 8c**).
269
270 **Live-sampling biases T cell activation by BMDMs**
271 Immunologically, the nature of sampling may have repercussion for how internalized antigens are presented
272 to T cells on Class I ('cross-presentation') versus Class II MHC. To examine how sampling through this
273 trogocytosis-like mechanism affects antigen presentation, we isolated ZsGreen^{+} BMDMs after co-culture
274 with DMSO- or Staurosoprine-treated B16F10 cell expressing ZsGreen fused to the OT-I and OT-II

275 ovalbumin (OVA) peptides (B16-ZsGminOVA)[13] (**Fig. 4n, Extended Data Fig. 9a**). We detected only
276 weak and indistinguishable activation in OT-II CD4 T cell activation after co-culture with BMDMs that
277 had acquired antigen through phagocytosis ("Phago-BMDMs") compared to those that had sampled live
278 cells ("Trogo-BMDMs") (**Fig. 4o, Extended Data Fig. 9b**). In contrast, Trogo-BMDMs but not Phago-
279 BMDMs induced significant OT-I CD8 T cell proximal activation (CD69 upregulation) and proliferation
280 (**Fig. 4p, Extended Data Fig. 9c**). This is consistent with the absence of trafficking of live-sampled material
281 to the degradative late endosome and lysosomal compartments and suggests a bias for cross-presentation.
282

283 **DISCUSSION**

284 Together, these findings demonstrate a substantial sampling of live cells that takes place via a trogocytosis-
285 like mechanism and which fills a distinct vesicular compartment that are particularly underrepresented in
286 late endosomes[10]. That macrophages can constitutively ingest small amounts of material from live cells is
287 in itself unsurprising; indeed a pruning function for macrophages has been demonstrated to be important to
288 activate stem cells[23] and to optimize brain circuitry via small synaptic pruning[24]. A key distinction here is
289 in understanding that this trogocytosis-like sampling may be undergoing at steady state in a variety of cells
290 and may be a significant source of self-antigen from healthy cells, giving macrophages a distinct
291 compartment with which to present healthy-self antigens, notably to CD8 T cells. We also note a single
292 previous suggestion of trogocytosis by dendritic cells which focused on a more conventional 'ripping'
293 mechanism leading to direct transfer of pre-formed peptide-MHC from the donor cell membrane[25]. In
294 contrast, using previously unavailable vesicle cytometry, our studies highlight the maintenance of sampled
295 material in a depot that can be processed by the APC for presentation. A more stable depot of self-antigens
296 provides a means of integrating and presenting the self-identity of many sampled cells, perhaps over days
297 or longer. The longer retention of material sampled by this trogocytosis-like mechanism may contribute to
298 a transferable pool of these vesicles, as have been observed to be exchanged amongst myeloid cells[13].
299 Ultimately, this work provides a novel framework to understand how the immune system can accumulate

300 information about our healthy-self: a system that then can tune T cells to the normal concentrations of self-
301 protein but may also be exploited by tumor cells to promote pathologic outcomes.
302

Acknowledgments: We thank all members of the Krummel lab for discussion and support. We acknowledge the UCSF Parnassus Flow Core CoLabs, particularly Vinh Nguyen and Tamara Roach, for assistance generating flow cytometry data (RRID: SCR_018206; DRC Center Grant NIH P30 DK063720) and the Biological Imaging Development Colab with assistance in data collection, instrumentation, and processing (NIH shared equipment grant S10OD028611-01). pCDH-puro-CMV-GC3AI was a gift from Binghui Li (Addgene plasmid # 78910; http://n2t.net/addgene:78910; RRID:Addgene_78910). This work was supported by R01 AI175277-01 and 2 R01 CA197363-06A1 to MFK. A.C.F. was supported by T32HL007185. R.T. was supported by T32AI007334. N.S. was supposed by the Human Frontier Science Program (LT000061/2018-L).

Author contributions:

A.C.F., R.T., N.S., K.M., M.R., and A.E. performed the experimental work. A.C.F., R.T., and M.F.K. wrote the manuscript with input from all authors. N.S. and M.F.K. conceived of the work.

Declaration of Interests: Authors declare no competing interests.

Supplementary Information is available for this paper.

320 **METHODS**

321 **RESOURCE AVAILABILITY**

322 ***Lead Contact***

323 Further information and requests should be directed to the Lead Contact: Matthew F. Krummel

324 (matthew.krummel@ucsf.edu).

325

326 ***Materials Availability***

327 Requests for resources and reagents should be directed to and will be fulfilled by the Lead Contact:

328 Matthew F. Krummel (matthew.krummel@ucsf.edu).

329

330 **EXPERIMENTAL MODEL AND SUBJECT DETAILS**

331

332 **Mice**

333 Mice were housed and bred under specific pathogen-free conditions at the University of California, San

334 Francisco Laboratory Animal Research Center and all experiments conformed to ethical principles and

335 guidelines approved by the UCSF Institutional Animal Care and Use Committee, the National Institutes of

336 Health and the American Association of Laboratory Animal Care. C57BL/6 and Ai16[26] ("mTmG") mice

337 were purchased from Jackson Laboratory or bred in house.

338 Both male and female mice ranging in age from 6 to 20 weeks were used for experimentation. Food and

339 water were provided ad libitum.

340

341 To generate ZsGreen reporter mice, Ai6 mice were crossbred with K14-Cre, Scgb1a1-Cre-ERT2, Villin-

342 Cre, B-actin-Cre mice. To induce ZsGreen expression in Scgb1a1-Cre-ERT2;Ai6 mice, mice were fed

343 tamoxifen-containing chow ad libitum for two weeks.

344

345 For tumor studies, B16-F10 melanoma cancer cells were resuspended in PBS and mixed at a1:1 (v:v) ratio

346 with growth factor reduced Matrigel Matrix (BD Biosciences) and 100000 cells in 50 uL were transplanted
347 into the subcutaneous region of the mouse flank. On day 14 after tumor challenge, when tumors reached a
348 size/volume of approximately 0.5 cm^3, mice were sacrificed, tumors were excised and processed for
349 downstream analysis.
350
351 **Tumor cell lines**
352 B16-F10 (ATCC, CRL-6475) was purchased. B16ZsGreen and B16ZsGreen minOVA cell lines were
353 described previously[13]. In brief, to make this cell line, B16-F10 melanoma parental cells were genetically
354 engineered using viral transduction with a ZsGreen or ZsGreen-minOVA construct. B16-GC3AI cell lines
355 were genetically engineered to stably express the GFP-Casp3-activity-indicator using viral transduction
356 with AddGene construct (Addgene #78910). Adherent cell lines were cultured at 37° C in 5% CO_2 in
357 DMEM (Invitrogen), 10% FCS (Benchmark), Pen/Strep/Glut containing 2 mM L-glutamine, 100 U/ml
358 penicillin, and 100 mg/ml streptomycin (Invitrogen).
359
360 **Mouse embryonic fibroblasts**
361 Mouse embryonic fibroblasts (MEFs) were derived from Ai6;B-actinCre mice that were generated by
362 crossing B-actin-Cre (strain # 033984, The Jackson Laboratory) to Ai6 mice (strain # 007906,The Jackson
363 Laboratory) as previously described[27]. Briefly, day 13.5 embryos were collected from pregnant females,
364 were minced, and digested with Trypsin. The retrieved cells were washed and plated in DMEM
365 (Invitrogen), 15% FCS (Benchmark), Pen/Strep/Glut (Invitrogen) for overnight culture at 37° C in 5% CO_2.
366 Media was aspirated after 24 h to remove any cells remaining in suspension and replaced with fresh media.
367 Cells were then grown to 70%–80% confluency and cryopreserved.
368
369

370 **METHOD DETAILS**

371 **Tissue digest and flow cytometry staining**

372 *Lung*

373 Lungs were collected from mice following euthanasia by overdose with 2.5% Avertin. Lungs were placed
374 in 3 mL of DMEM (Gibco) in C-Tubes (Miltenyi) briefly processed with a GentleMACS Dissociator
375 (Miltenyi). 2 mL of DMEM with 0.26 U/mL LiberaseTM (Roche) and 0.25 mg/mLDNase I (Roche) was
376 subsequently added and samples were then incubated at 37° C in a shaker for 30 min and dissociated to
377 single cell suspensions by GentleMACS. Tissue homogenate was then passed through a 100 mm filter. Red
378 blood cells were lysed with 3 mL of RBC Lysis Buffer (155 mM NH4Cl, 12 mM NaHCO3, 0.1 mM EDTA)
379 per lung for 5 min at room temperature. Samples were then washed with FACS buffer (2% FBS, 2mM
380 EDTA in PBS) and resuspended in appropriate buffer for staining for flow cytometry or FACS.

381

382 *Tumor*

383 For tumor digests, tumors from mice were harvested 14 days after injection. Tumors were minced and
384 incubated in digestion buffer (100 U/mL collagenase type I (Roche), 500 U/mL collagenase type IV
385 (Roche), and 200 mg/mL DNAse I (Roche) in RPMI1640 (Gibco)) for 30 minutes on a shaker at 37 ^{o} C.
386 Digestion mixtures were then pipetted repeatedly, followed by a second 15-minute incubation at 37° C.
387 Cells were quenched with RPMI-1640 (GIBCO) plus 10% FCS, washed with FACS buffer, and filtered
388 through a 100-mm cell strainer before staining for flow cytometry.

389

390 *Lymph Nodes*

391 Inguinal lymph nodes (LN) were dissected from mice, cleaned of fat, and digested as previously described
392 [14]. In brief, LN were pierced and torn with sharp forceps in 24-well plates and incubated for 15 min at 37°
393 C in 1 ml digestion buffer (100 U/ml collagenase type I (Roche), 500 U/ml collagenase type IV (Roche),
394 and 20 μg/ml DNAse I (Roche) in RPMI-1640 (GIBCO)). Cells were pipetted up and down repeatedly,

395 followed by a second 15-minute incubation at 37° C. After digestion, LN were washed with RPMI-1640
396 (GIBCO) plus 10% FCS, washed with FACS buffer, and filtered through 70 μm Nytex filters before staining
397 for flow cytometry.
398
399 **Imaging Sample Preparation, Image Acquisition, and Image Analysis**
400 *Two photon imaging of mouse lung, skin, tumor, and gut slices.*
401 Imaging of lung, skin, tumor, and gut slices were performed using a custom-built two-photon setup
402 equipped with two infrared lasers (MaiTai: Spectra Physics; Chameleon: Coherent). The Chameleon laser
403 was set to 950nm for excitation of ZsGreen. Emitted light was detected using a 25x 1.2NA water lens
404 (Zeiss) coupled to a 6-color detector array (custom; using Hamamatsu H9433MOD detectors). Emission
405 filters used were blue 475/23, green 510/42, yellow 542/27, red 607/70, far red 675/67. The microscope
406 was controlled by the MicroManager software suite, and time-lapse z stack images were acquired every 90
407 s with five-fold averaging and z-step of 4mm. Data analysis was performed with Imaris software (Bitplane).
408 For lung slices, mice were euthanized by anesthetic overdose with 1 mL 2.5% Avertin and then
409 intubated by tracheotomy with the sheath from an 18-gauge i.v. catheter. Lungs were subsequently inflated
410 with 1 mL of 2% low melting agarose (BMA) in sterile PBS at 37C. Agarose was then solidified by flooding
411 the chest cavity with 4C PBS. Inflated lungs were excised, and the left lobe was cut into 300mm sections
412 using a vibratome. For skin, tumor, and gut slices, mice were euthanized using CO2, obstructing fat was
413 removed, and tissue sections were embedded in 4% low-melting agarose in PBS prior to sectioning.
414 Sections were mounted on plastic coverslips and imaged by two-photon microscopy at 37C in carbogen
415 (5% CO2:95% O2)-perfused RPMI-1640 media (GIBCO, without Phenol Red) in a heated chamber.
416
417 *Spinning Disk Confocal*

418 Glass bottom 96 well plates were coated in fibronectin and washed as described above. Sorted ZsGreen+
419 BMDMs after antigenic transfer or unsorted antigenic transfer assays were imaged. Spinning disk confocal
420 was performed at 37°C with a 488 and 561 nm lasers with 40% and 50% laser powers, respectively.
421
422 *Nikon NSPARC*
423 Glass bottom 96 well flat bottom plates were coated with 50ug/mL fibronectin in H_2O at 37°C for 1 h, or
424 at 4°C overnight, before use. Fibronectin coated wells were washed 2x with PBS prior to use. $8x10^3$
425 TdTomato+ BMDMs were plated with $1.2x10^4$ ZsGreen+ B16F10s or ZsGreen+ MEFs and spun at 1500g
426 for 5 min. Cells were incubated at 37°C for 2 hours prior to imaging. NSPARC imaging was performed at
427 37°C with 488 and 560 nm lasers with 1.0% and 2.0% laser powers, respectively.
428
429 *Lattice light-sheet microscopy*
430 5 mm round coverslips were cleaned by a plasma cleaner and coated with 2 µg/ml fibronectin in H_2O at
431 37°C for 1 h, or at 4°C overnight, before use. Fibronectin coated coverslips were washed 2x with PBS prior
432 to use. Cells were plated onto fibronectin-coated coverslips 20 min prior to imaging with a 10 min spin at
433 1,400 rpm and 4°C. Coverslip was immediately loaded into the sample bath with warmed imaging media
434 and secured. Imaging was performed at 37°C with a 488 and 560 nm laser (MPBC). Exposure time was 10
435 ms per frame leading to a temporal resolution of ~4.5. LLS microscope was a homebuilt clone of the scope
436 described by Chen et al.[28] with a Nikon CFI Apo LWD 25× W 1.1 NA 2 mm working distance objective,
437 Hamamatsu Orca Flash 4.0 v2 camera, and Custom LabView acquisition software. Method was derived
438 from previous work[19].
439
440 *Image Analysis*
441 All computational image analysis was performed in Imaris version 9.9.1 or 10.2.0 (Bitplane) and Fiji
442 version 2.16.0/1.54p. Particle area analysis was performed using the Analyze particles function in Fiji with

443 the following parameters: size (.027- infinity) and circularity (0.00-1.00). Post processing raw data from
444 lattice light-sheet images were deconvoluted using iterative Richardson-Lucy deconvolution as
445 implemented in LLSpy. Briefly, images were deconvolved with a known point spread function that was
446 recorded for each color prior to the experiment, as described previously[19]. A typical sample area underwent
447 15-20 iterations of deconvolution. For live imaging experiments, photobleaching correction was applied in
448 FIJI using the histogram matching method. Particle volume was measured using the object-object statistics
449 function in Imaris from the separated vesicle in frames 13-18.
450

451 **Flow cytometry and fluorescence-activated cell sorting**

452 Zombie NIR Fixable Viability Kit (#423106; BioLegend), DAPI, or PI was used for exclusion of dead cells.
453 Surface staining was performed with anti-mouse Fc receptor antibody (clone 2.4G2, UCSF Hybridoma
454 Core) in FACS buffer for 30 min on ice. Supplementary Table 1 lists all antibodies referenced for flow
455 cytometry and imaging experiments. For all experiments involving intracellular staining, BD
456 Cytofix/Cytoperm (#554722) was used. Following fixation and permeabilization, cells were incubated with
457 Fc block for 10 min on ice prior to addition of intracellular stain. Flow cytometry was performed on a BD
458 Fortessa instrument, and sorting was performed on BD FACSAria or BD FACSAria Fusion instruments.
459 FlowJo software (BD Biosciences) was used for all analyses.
460

461 **Generation of BMDMs**

462 6-12 week old C57BL/6 mice were euthanized and their femurs and tibiae were excised. Bone marrow was
463 crushed using a mortar and pestle. After pelleting the bone marrow, the red blood cells were lysed using
464 RBC lysis buffer for 5 min at RT. Cells were washed with FACS buffer and filtered through a 100 mm cell
465 strainer before being seeded at 1x106 cells / mL on a low-adherent cell culture dish in BMDM media
466 (DMEM supplemented with 10% FBS (Benchmark), 50 mM beta-mercaptoethanol, Pen/Strup/Glut

467 (Invitrogen), and 20 ng/ml M-CSF (Peprotech)). Fresh BMDM media was added on day 3-4 of culture. On
468 day 6-7 of culture, BMDMs were harvested and used for experiments.
469
470 **In vitro antigen transfer assay**
471 BMDMs were isolated as described above from wildtype C57BL/6 and co-cultured with target B16-
472 ZsGreen cells or MEF-ZsGreen cells at a 1:1 ratio for 16 hours before assays unless otherwise noted. Cells
473 were plated in BMDM media in low-adherent 96 well flat-bottom plates prior to staining and analysis by
474 flow cytometry.
475
476 **Drug/Inhibitor antigenic transfer assay**
477 Antigenic transfer assays were performed as described above. For all experiments wherein apoptosis was
478 induced, B16F10 cells or MEFs were treated with Staurosporine and washed with PBS prior to antigenic
479 transfer assays. For exosome/microparticle inhibitory experiments DMA or Calpeptin were plated at 0 h to
480 a final concentration of 10mM and 20mM, respectively. For endocytic inhibition experiments Dynasore
481 was plated at 0 h to a final concentration of 20mM. Caspase inhibition was performed using zVAD at a
482 final concentration of 20mM at 0 h.
483
484 **Supernatant/transwell antigenic transfer assay**
485 Media was replaced on B16-ZsGreen cells or MEF-ZsGreen cells upon reaching 80% confluency. After 48
486 h supernatants were collected and used in antigenic transfer assays as described above. Transwell
487 experiments were performed as described in antigen transfer assays with a 3um pore transwell insert
488 separating BMDM and ZsGreen+ target cells or supernatants.
489
490 **Antibody Opsonization and Blockade**

491 For opsonization experiments, B16-ZsGreen or MEF-ZsGreen target cells were pre-coated with 10ug/mL
492 Armenian Hamster IgG (BD Pharmigen, Cat# 553969), 10ug/mL Rat IgG2ak (clone 2A3, invivoMab Cat#
493 BE0089), 10ug/mL CD29 (eBioHmb1-1, eBioscience Cat #16-0291-85), 10ug/mL aCD98 (RL388,
494 Biolegend Cat# 128202), normal mouse serum (Jackson ImmunoResearch
495 Cat# 015-000-120), or 500ug/mL IgG from normal mouse serum at 37C for 30-60 minutes and washed with
496 PBS prior to co-culture with BMDMs. IgG from normal mouse serum was isolated using Protein G
497 dynabeads (Invitrogen Cat# 10003D) according to manufacturer instructions and dialyzed with PBS (Slide-
498 A-Lyzer). Concentration of isolated IgG was quantified using IgG ELISA (abcam, Cat # ab151276).
499 For antibody blockade, BMDMs were pre-treated with 10ug/mL Rat IgG2b (clone MPC-11, invivoMab
500 BE0086) or CD11b-blocking antibody (clone M17/0, Biolegend Cat# 101202) for 1 hour before 16-hour
501 co-culture antigen transfer assays.
502

503 **CRISPR Editing of Primary BMDMs**

504 CRISPR editing of primary BMDMs were performed as previously described[29]. Briefly, sgRNA targeting
505 *Rosa26 (ACUCCAGUCUUUCUAGAAGA)*, *Itgam (GAAGCCAUGACACAAGGCUA)*, and *Itgb2*
506 (*CUCUAGAACUUCACUGGACC*) were ordered from Synthego and reconstituted to 100uM in TE (IDT).
507 sgRNA and Cas9 (6.5mg/mL) was complexed in a 2:1 molar ratio at room temperature for at least 10
508 minutes. At 3 days after initial plating, BMDM differentiation cultures were harvested, and cells were
509 washed with PBS prior to electroporation with ribonucleoprotein (RNP) containing gene-targeting sgRNA
510 complexed in P3 primary cell solution with electroporation code CM137 using the Lonza 4D Nucleofector.
511 After an additional 4 days of differentiation, gene-edited BMDMs were either stained with antibodies for
512 validation of protein knockdown or co-cultured with ZsGreen target cells for 16 hours before evaluated by
513 flow cytometry.
514

515 **Vesicle Flow Cytometry**

516 *Sample Preparation and Sorting*

517 16 hours prior to sorting, BMDMs were cultured with live target cells ("Trogocytosis") in a 1:1 ratio,
518 Staurosporine-treated target cells ("Phagocytosis") in a 1:1 ratio, or supernatant derived from target cells
519 ("Endocytosis"). Cells were harvested, washed with FACS buffer, stained with CD45-BUV395 with
520 FcBlock for 30 minutes on ice, washed with FACS buffer, and resuspended in FACS buffer + 1 mg/mL PI
521 at 10E6 cells/mL. CD45+ cells were sorted on FACSAria and FACSFusion machines on "Purity" into
522 FACS buffer kept at 4C.

523

524 *Surface Biotinylation and Lysis*

525 Cells were washed 3x in PBS, resuspended in PBS at 25E6 cells/mL then biotinylated with 80 uL of 10mM
526 EZ-Link Sulfo-NHS-SS-Biotin (ThermoFischer Scientific #21331) per mL of reaction volume for 30
527 minutes at 4C. Cells were washed 3x in PBS, resuspend in at least 500 uL homogenization buffer (250mM
528 sucrose, 200mM PMSF, 250mM sucrose, 3mM Imidazole, 1X protease inhibitor filtered through 0.1um
529 filter) at a concentration of 10E6 cells/mL, and drawn 15 times up and down through a 22G needle. Cell
530 homogenate was spun for 4 minutes at 150xg, and post-nuclear supernatant was spun at 3000xg for 5 min
531 at 4C to collect vesicles.

532

533 *Staining*

534 All staining reagents were filtered using a 0.1um filter prior to use and vesicles were pelleted using spin
535 speeds of 3000xg for 5 min at 4C for all steps. Vesicles were stained with 50uM CellTrace Violet
536 (ThermoFischer Scientific Cat# C34557) for 5 minutes at room temperature and washed once with PBS.
537 Samples were fixed for 20 minutes at room temperature with fixation buffer (Invitrogen Cat# 88-8824-00),
538 washed with permeabilization buffer (Invitrogen Cat# 88-8824-00) twice, and stained in 50 uL of
539 permeabilization buffer with 1% FCS with FcBlock for 30 minutes at room temperature. Vesicles were
540 washed with permeabilization buffer and resuspend in 100 uL PBS for acquisition.

541

542 *Sample Acquisition and Analysis*

543 Aurora Cytek flow cells were soaked with contrad overnight with long clean prior to acquisition with
544 filtered reagents. Calibration beads and samples were acquired on the Aurora Cytek with Enhanced Small
545 Particle detection.

546

547 **T cell stimulation assays**

548 ZsGreen+ BMDMs were sorted from BMDM 16-hour co-cultures with DMSO- or Staurosporine-pretreated
549 B16zsGreenminOVA. To induce MHC II expression on BMDMs, sorted cells were stimulated with
550 20ng/mL IFNg for 2 hours and then washed prior to co-culture with T cells. OTI and OTII T cells were
551 isolated from spleens of TCR transgenic mice after RBC lysis using either a CD8 or CD4 EasySep
552 enrichment kit (STEMCELL Technologies), respectively. T cells were labeled with CellTraceViolet
553 (ThermoFischer Scientific) at 37C in PBS for 15 minutes and washed in RPMI prior to use. T cell
554 stimulation assay was performed as previous described. Briefly, sorted BMDMs and T cells were added to
555 the wells of a 96-well V-bottom plate at a 1:3 ratio in RPMI (Gibco) supplemented with 10% FCS
556 (Benchmark), Pen/Strep/Glut (Invitrogen), and 50 mM beta-mercaptoethanol (Thermo Fisher). Cells were
557 harvested for analysis 3 days later. Dilution of cell permeable dye CellTraceViolet and expression of CD69
558 were used as indicators of T cell stimulation.

559

560 **QUANTIFICATION AND STATISTICAL ANALYSIS**

561 **Statistical analysis**

562 Unless specifically noted, all data are representative of >3 separate experiments. Experimental group
563 assignment was determined by genotype or, if all WT mice, by random designation. Statistical analyses
564 were performed using GraphPad Prism software. Error bars represent standard error of the mean (S.E.M.)
565 calculated using Prism, and are derived from triplicate or greater experimental conditions. Specific

566 statistical tests used were paired and unpaired t-tests and p values <0.05 were considered statistically
567 significant. For pairwise comparisons, unpaired t tests were used unless otherwise noted. For statistical
568 measures between more than two groups, one-way ANOVA would be performed unless otherwise noted.
569 Investigators were not blinded to group assignment during experimental procedures or analysis.
570

571 **DATA AVAILABILITY**

572 The data reported are in the Article and its associated Supplementary, and all relevant data are available
573 from the corresponding author on request.

574 **REFERENCES**

575 1. Medawar, P.B. (1961). IMMUNOLOGICAL TOLERANCE.

576 2. Goodnow, C.C., Sprent, J., de St Groth, B.F., and Vinuesa, C.G. (2005). Cellular and genetic
577 mechanisms of self tolerance and autoimmunity. Nature *435*, 590–597.
578 https://doi.org/10.1038/nature03724.

579 3. Kamradt, T., and Mitchison, N.A. (2001). Tolerance and Autoimmunity. N. Engl. J. Med. *344*, 655–
580 664. https://doi.org/10.1056/NEJM200103013440907.

581 4. Kenison, J.E., Stevens, N.A., and Quintana, F.J. (2023). Therapeutic induction of antigen-specific
582 immune tolerance. Nat. Rev. Immunol., 1–20. https://doi.org/10.1038/s41577-023-00970-x.

583 5. Cummings, R.J., Barbet, G., Bongers, G., Hartmann, B.M., Gettler, K., Muniz, L., Furtado, G.C.,
584 Cho, J., Lira, S.A., and Blander, J.M. (2016). Different tissue phagocytes sample apoptotic cells to direct
585 distinct homeostasis programs. Nature *539*, 565–569. https://doi.org/10.1038/nature20138.

586 6. Kushwah, R., Wu, J., Oliver, J.R., Jiang, G., Zhang, J., Siminovitch, K.A., and Hu, J. (2010). Uptake
587 of apoptotic DC converts immature DC into tolerogenic DC that induce differentiation of Foxp3+ Treg.
588 Eur. J. Immunol. *40*, 1022–1035. https://doi.org/10.1002/eji.200939782.

589 7. Myers, D.R., Zikherman, J., and Roose, J.P. (2017). Tonic Signals: Why do Lymphocytes Bother?
590 Trends Immunol. *38*, 844–857. https://doi.org/10.1016/j.it.2017.06.010.

591 8. Stefanová, I., Dorfman, J.R., and Germain, R.N. (2002). Self-recognition promotes the foreign
592 antigen sensitivity of naive T lymphocytes. Nature *420*, 429–434. https://doi.org/10.1038/nature01146.

593 9. Hogquist, K.A., and Jameson, S.C. (2014). The self-obsession of T cells: how TCR signaling
594 thresholds affect fate "decisions" and effector function. Nat. Immunol. *15*, 815–823.
595 https://doi.org/10.1038/ni.2938.

596 10. Blum, J.S., Wearsch, P.A., and Cresswell, P. (2013). Pathways of Antigen Processing. Annu. Rev.
597 Immunol. *31*, 443–473. https://doi.org/10.1146/annurev-immunol-032712-095910.

598 11. Greene, J.T., Brian, B.F., Senevirathne, S.E., and Freedman, T.S. (2021). Regulation of myeloid-cell
599 activation. Curr. Opin. Immunol. *73*, 34–42. https://doi.org/10.1016/j.coi.2021.09.004.

600 12. White, S.R. (2011). Apoptosis and the Airway Epithelium. J. Allergy *2011*, 948406.
601 https://doi.org/10.1155/2011/948406.

602 13. Ruhland, M.K., Roberts, E.W., Cai, E., Mujal, A.M., Marchuk, K., Beppler, C., Nam, D., Serwas,
603 N.K., Binnewies, M., and Krummel, M.F. (2020). Visualizing Synaptic Transfer of Tumor Antigens
604 among Dendritic Cells. Cancer Cell *37*, 786-799.e5. https://doi.org/10.1016/j.ccell.2020.05.002.

605 14. Roberts, E.W., Broz, M.L., Binnewies, M., Headley, M.B., Nelson, A.E., Wolf, D.M., Kaisho, T.,
606 Bogunovic, D., Bhardwaj, N., and Krummel, M.F. (2016). Critical Role for CD103+/CD141+ Dendritic
607 Cells Bearing CCR7 for Tumor Antigen Trafficking and Priming of T Cell Immunity in Melanoma.
608 Cancer Cell *30*, 324–336. https://doi.org/10.1016/j.ccell.2016.06.003.

609 15. Pham, T., Mero, P., and Booth, J.W. (2011). Dynamics of Macrophage Trogocytosis of Rituximab-
610 Coated B Cells. PLOS ONE *6*, e14498. https://doi.org/10.1371/journal.pone.0014498.

611 16. Blander, J.M. (2017). The many ways tissue phagocytes respond to dying cells. Immunol. Rev. *277*,
612 158–173. https://doi.org/10.1111/imr.12537.

613 17. Yin, C., and Heit, B. (2021). Cellular Responses to the Efferocytosis of Apoptotic Cells. Front.
614 Immunol. *12*. https://doi.org/10.3389/fimmu.2021.631714.

615 18. Zhang, J., Wang, X., Cui, W., Wang, W., Zhang, H., Liu, L., Zhang, Z., Li, Z., Ying, G., Zhang, N., et
616 al. (2013). Visualization of caspase-3-like activity in cells using a genetically encoded fluorescent
617 biosensor activated by protein cleavage. Nat. Commun. *4*, 2157. https://doi.org/10.1038/ncomms3157.

618 19. Cai, E., Marchuk, K., Beemiller, P., Beppler, C., Rubashkin, M.G., Weaver, V.M., Gérard, A., Liu,
619 T.-L., Chen, B.-C., Betzig, E., et al. (2017). Visualizing dynamic microvillar search and stabilization
620 during ligand detection by T cells. Science *356*, eaal3118. https://doi.org/10.1126/science.aal3118.

621 20. Hong, S., Beja-Glasser, V.F., Nfonoyim, B.M., Frouin, A., Li, S., Ramakrishnan, S., Merry, K.M.,
622 Shi, Q., Rosenthal, A., Barres, B.A., et al. (2016). Complement and microglia mediate early synapse loss
623 in Alzheimer mouse models. Science *352*, 712–716. https://doi.org/10.1126/science.aad8373.

624 21. Hoffmann, E., Pauwels, A.-M., Alloatti, A., Kotsias, F., and Amigorena, S. (2016). Analysis of
625 Phagosomal Antigen Degradation by Flow Organellocytometry. BIO-Protoc. *6*.
626 https://doi.org/10.21769/BioProtoc.2014.

627 22. Song, W., Cho, H., Cheng, P., and Pierce, S.K. (1995). Entry of B cell antigen receptor and antigen
628 into class II peptide-loading compartment is independent of receptor cross-linking. J. Immunol. *155*,
629 4255–4263. https://doi.org/10.4049/jimmunol.155.9.4255.

630 23. Wattrus, S.J., Smith, M.L., Rodrigues, C.P., Hagedorn, E.J., Kim, J.W., Budnik, B., and Zon, L.I.
631 (2022). Quality assurance of hematopoietic stem cells by macrophages determines stem cell clonality.
632 Science *377*, 1413–1419. https://doi.org/10.1126/science.abo4837.

633 24. Weinhard, L., di Bartolomei, G., Bolasco, G., Machado, P., Schieber, N.L., Neniskyte, U., Exiga, M.,
634 Vadisiute, A., Raggioli, A., Schertel, A., et al. (2018). Microglia remodel synapses by presynaptic
635 trogocytosis and spine head filopodia induction. Nat. Commun. *9*, 1228. https://doi.org/10.1038/s41467-
636 018-03566-5.

637 25. Harshyne, L.A., Zimmer, M.I., Watkins, S.C., and Barratt-Boyes, S.M. (2003). A Role for Class A
638 Scavenger Receptor in Dendritic Cell Nibbling from Live Cells. J. Immunol. *170*, 2302–2309.
639 https://doi.org/10.4049/jimmunol.170.5.2302.

640 26. Muzumdar, M.D., Tasic, B., Miyamichi, K., Li, L., and Luo, L. (2007). A global double-fluorescent
641 Cre reporter mouse. genesis *45*, 593–605. https://doi.org/10.1002/dvg.20335.

642 27. Headley, M.B., Bins, A., Nip, A., Roberts, E.W., Looney, M.R., Gerard, A., and Krummel, M.F.
643 (2016). Visualization of immediate immune responses to pioneer metastatic cells in the lung. Nature *531*,
644 513–517. https://doi.org/10.1038/nature16985.

645 28. Chen, B.-C., Legant, W.R., Wang, K., Shao, L., Milkie, D.E., Davidson, M.W., Janetopoulos, C., Wu,
646 X.S., Hammer, J.A., Liu, Z., et al. (2014). Lattice light-sheet microscopy: imaging molecules to embryos
647 at high spatiotemporal resolution. Science *346*, 1257998. https://doi.org/10.1126/science.1257998.

648 29. Freund, E.C., Lock, J.Y., Oh, J., Maculins, T., Delamarre, L., Bohlen, C.J., Haley, B., and Murthy, A.
649 (2020). Efficient gene knockout in primary human and murine myeloid cells by non-viral delivery of
650 CRISPR-Cas9. J. Exp. Med. *217*, e20191692. https://doi.org/10.1084/jem.20191692.

651

652